ISSN: 2096-3246
Volume 58, Issue 01, 2026

TITLE: DEVELOPMENT AND STUDY OF ENHANCED GAMMA RAY SHIELDING PROPERTIES OF NOVEL SILVER OXIDE DOPED BISMUTH BORO-TELLURITE GLASSES.

R. Praveen Kumar[a, *], Susheela K. Lenkennavar[a, **]
[a] Department of Physics, Bangalore University, Bengaluru, Karnataka, 560105, India.
[a] Department of Physics, Bangalore University, Bengaluru, Karnataka, 560056, India.
*e-mail: vyasa8273praveen@gmail.com
**Correspondance author e-mail: susheelakl@bub.ernet.in

Abstract

This work analyzes a glass sample with the chemical formula (65-x)B_2O_3-15TeO_2-15Bi_2O_3-5La_2O_3-xAg_2O, where x equals 0, 0.5, 1, 1.5, and 2 mol%. The density of the glass samples increased from 3.15 to 3.2 g/cm³, and the molar volume also increased from 49.326 to 49.56 cm^3/mole, with increasing molar concentration of Ag_2O. The linear attenuation coefficients were calculated for gamma photons over the energy range 015MeV – 15 MeV. With these linear attenuation coefficient values, further attenuation parameters, i.e., half value layer (HVL), mass attenuation coefficient (MAC), and effective atomic number (Z_{eff}), were then calculated. The measured values of these attenuation parameters were also compared with the theoretical values obtained through the online software Py-MLBUF. The findings show that the linear attenuation coefficient (LAC) increases with increasing sample density and increasing proportions of Ag_2O. The prepared glasses indicate a stronger shielding ability among the materials investigated than the usual glass and concrete samples do. This study highlights the potential of these glass compositions as effective materials for gamma radiation shielding.

Keywords: Mass attenuation coefficient, radiation shielding, linear attenuation coefficient, effective atomic number, silver oxide, photon energy.

1. Introduction

Radiation shielding materials play crucial roles in safeguarding human health and the environment from the harmful effects of ionizing radiation [1]. High-density substances and heavy elements, such as lead, are particularly effective at absorbing this type of radiation. However, the use of lead presents several significant challenges. Its toxicity poses health risks, but its substantial weight and bulkiness can complicate its handling and installation in various applications. Additionally, the opaque nature of lead limits visibility, which can be a disadvantage in settings where transparency is desired. As a result, alternative shielding materials that can provide adequate protection without the drawbacks associated with lead are needed. Protective shields are one of the primary techniques for lowering radiation intensity and, as a result, reducing radiation risk. Radiation shielding consists of the use of physical barriers such as lead, aluminum, concrete, and other materials [2-5].

Radiation shielding concrete provides essential protection against harmful radiation across a range of applications, making it a valuable material in industries such as nuclear energy and

medical facilities. Its effectiveness in absorbing and attenuating radiation makes it a preferred choice for constructing barriers and protective structures. Despite its advantages, radiation shielding concrete is not without its limitations. Factors such as weight, cost, and potential for cracking under certain conditions, thermal insulation, maintenance, durability, and others can pose challenges in its use. Additionally, the specific requirements for radiation shielding may necessitate careful consideration of the composition and thickness of the concrete, which can complicate the design and implementation processes.

Radiation shielding, often referred to as radiological protection, is determined by a material's capacity to decrease the quantity of incoming photons and their energy levels. This capability is crucial in various applications where radiation exposure is a concern. Understanding how different materials interact with photons allows for the development of effective shielding solutions. The interactions between photons and the atoms of the shielding material primarily cause a decrease in photon energy. Thus, for a material to be classified as an efficient and robust radiation-shielding solution, it must incorporate elements with higher atomic numbers, possess a high density, and demonstrate excellent thermal and structural properties. Additionally, it should be thin and economically feasible to ensure its effectiveness [6-9]. Glass materials present a viable alternative to traditional substances such as lead and concrete, primarily due to their unique physical and optical characteristics, which can be tailored through variations in composition and preparation methods [10]. The versatility of glass allows for adjustments in its refractive index, transparency, and strength, making it suitable for a wide range of applications, from construction to advanced optics. This highlights the potential of glass to meet specific performance criteria while also addressing environmental concerns associated with the use of lead and concrete. By leveraging innovative glass formulation and processing techniques, it is feasible to develop materials that meet structural standards while improving visual appeal and functionality across different environments.

An evaluation has been conducted on various binary, ternary, and polyborate glasses to determine their structural and γ–RS properties. The studies conducted by [11] and [12] focused on the γ–RS characteristics of zincborate glasses. In addition [13] examined various glass systems that incorporate rare earth oxides such as Y_2O_3 (Yttrium oxide), Gd_2O_3 (Gadolinium oxide), $NdCl_3$ (Neodymium oxide), PrO_{11} (Praseodymium oxide), and Dy_2O_3 (Dysprosium oxide). In addition, [14] analyzed the role of bismuth oxide in the γ–RS characteristics of binary and ternary glasses via theoretical and computational approaches [3]. Examining the glasses for radiation protection is appropriate considering the facts and figures presented. Thus, it is logical and worthwhile to investigate bismuth–Boro tellurite glasses doped with Ag_2O through an analysis of gamma shielding by varying the concentration of silver oxide.

Owing to their toxic nature, lead-based glasses are declining in popularity. Recent research has focused on developing heavy metal oxide glasses, particularly tellurite glasses, for use in radiation shielding applications. Tellurite glasses are increasingly sought as radiation shielding materials because of their advantageous properties, including nontoxicity, high density, elevated refractive index, and excellent chemical resistance. These characteristics make them promising alternatives in various applications where safety and effectiveness are paramount.

Several studies suggest that tellurite glasses have a considerable ability to shield against radiation. The effectiveness of these glasses can be further increased by incorporating WO_3 or B_2O_3, thereby improving their radiation protection performance. These findings highlight the potential of tellurite glasses in applications requiring radiation shielding, suggesting that modifications with specific additives can optimize their performance. These advancements could lead to more efficient materials for various industrial and medical uses. Compared with those of borotellurite glasses, the mechanical, optical, chemical, and thermal features of a borotellurite glass system are enhanced [15].

The presence of lead in various materials can lead to a range of serious health issues, including damage to the kidneys and brain, increased risk of miscarriages, and disturbances in the nervous system. Recognizing these dangers, both the International Agency for Research on Cancer (IARC) and the Department of Health and Human Services (DHHS) have classified lead and its compounds as environmental toxins and likely carcinogens for humans [16]. In light of these significant health risks, developing alternative materials has become crucial. Boro tellurite glasses doped with bismuth, vanadium, and silver have emerged as promising substitutes for lead in creating radiation shielding materials. These innovative glasses mitigate the harmful effects of lead and provide adequate protection against radiation, thereby contributing to safer environments in various applications. The inclusion of certain transition metal oxides (ZnO, CaO, Al_2O_3, SrO, Ag_2O, and SnO) and rare earth oxides (Gd_2O_3, Sm_2O_3, and La_2O_3) in the glass composition is advantageous, as these oxides function as modifiers in the glass-making process. Specifically, the presence of Ag_2O enhances the optical performance and radiation protection of glass [17, 18]. The fundamental gamma-ray shielding attributes were analyzed, focusing on the effective atomic number (Z_{eff}), electron density (N_{eff}), half-value layer (HVL), linear attenuation coefficient (LAC, μ), mass attenuation coefficient (MAC,μ_m), and mean free path (MFP, λ). The glass compositions explored in this study include boro-tellurite, silver, bismuth, and lanthanum.

Formulated explicitly as $(65\text{-}x)B_2O_3\text{-}15TeO_2\text{-}15Bi_2O_3\text{-}5La_2O_3\text{-}xAg_2O$, the variable x can take 0, 0.5, 1, 1.5, and 2 mol% values. This composition highlights the intricate balance of various oxides, with boron oxide (B_2O_3) serving as the primary component. In contrast, tellurium oxide (TeO_2), bismuth oxide (Bi_2O_3), lanthanum oxide (La_2O_3), and silver oxide (Ag_2O) contribute to the overall properties of glass. A detailed analysis of the elemental composition is available in Table 1, which serves as a reference point for understanding the specific ratios and functions of each oxide in the formation and characteristics of the glass system. This careful selection of components is crucial for tailoring the material's optical, physical, and radiation properties, making it suitable for various applications in materials science.

The densities (ρ) of the glasses were assessed via a density model [19]. Additionally, each sample's molar volume (V_m) was calculated, with the corresponding values of ρ and V_m presented in Table 1. These measurements provide essential insights into the physical properties of the glasses, facilitating further analysis and comparison among the samples. The following formula calculates the glasses' theoretical density (ρ) values [19]. was utilized.

$$\rho = 0.53.\frac{\sum M_i X_i}{\sum V_i X_i} + 0.35\ldots\ldots \quad \text{for Binary and Tertiary} \qquad (1)$$

$\rho = 0.53.\frac{\sum M_i X_i}{\sum V_i X_i} + 0.75$……. For Quaternary, Senary, e.t.c

Table 1. Chemical Composition and density of (65-x)B_2O_3-15TeO_2-15Bi_2O_3-5La_2O_3-xAg_2O**,** where x = 0, 0.5, 1, 1.5, 2 mol%

Sample Code	Chemical Composition (mol%)					Density (g/cm^3)	Molar Volume (cm^3/mol)
	B_2O_3	TeO_2	Bi_2O_3	La_2O_3	Ag_2O		
BBTLA0	65	15	15	5	0	3.15	49.326
BBTLA0.5	64.5	15	15	5	0.5	3.16	49.426
BBTLA1	64	15	15	5	1	3.18	49.370
BBTLA1.5	63.5	15	15	5	1.5	3.19	49.47
BBTLA2	63	15	15	5	2	3.2	49.56

2. computational background

2.1.Theoretical calculations via Phys-X software

Phy-X software was used to estimate the radiation shielding factors for the BBTLA samples. Phy-X software [20], effectively estimates radiation shielding factors for various glass systems. It is particularly valuable for assessing the shielding capabilities of materials against both low and high-energy photons. One of the key advantages of Phy-X is its user-friendly interface, which allows for straightforward input of the glass composition and density on the main page [21]. This simplicity, combined with the program's accuracy, makes it an essential resource for researchers and professionals in the field. Users can input the glass composition in either mol% or wt%, and the density should be provided in g/cm^3. Additionally, it is necessary for the user to select the energy range for testing the samples. In this analysis, energies were specified within the range of 0.015 MeV to 15 MeV.

2.2.Py-MLBUF software

A new convenient online software for photon shielding parameter calculations was also established by Mann & Mann. The Py-MLBUF is an intuitive online platform designed to calculate gamma-ray shielding parameters. It efficiently computes 36 distinct parameters across an energy range of 0.015 MeV to 15 MeV, making it a valuable tool for professionals in the field [22]. This user-friendly interface simplifies the complex gamma ray shielding analysis process, allowing users to easily obtain precise calculations. By leveraging this

platform, users can enhance their understanding and application of gamma-ray shielding in various contexts.

Typically, various essential parameters are assessed via software such as Phy-X/PSD and Py-MLBUF to explore the feasibility of utilizing glassy materials in diverse nuclear applications, particularly for radiation shielding. These applications yield precise measurements of shielding factors, including the mass attenuation coefficient (MAC), half value thickness (HVT), effective atomic number (EAN), and linear attenuation coefficient (LAC). For the produced BBTLAg0, BBTLAg0.5, BBTLAg1, BBTLAg1.5, and BBTLAg2 glasses, the Phy-X/PSD program was employed to calculate shielding factors across multiple energy levels ranging from 0.015 M eV to 15 MeV, and these values were compared with those obtained from Py-MLBUF.

2.3.Analysis of radiation shielding capabilities

As a fundamental shielding parameter, the linear attenuation coefficient (LAC) indicates the capacity of a material to attenuate incident radiation. The linear attenuation coefficient (μ) can be utilized to measure the interaction of gamma rays with materials,

The linear attenuation coefficient (LAC, in cm^{-1}) serves as a crucial parameter for evaluating the effectiveness of shielding materials in reducing incident radiation. This coefficient quantifies how well a specific material can decrease the radiation intensity as it passes through. Experimental methods can be employed to determine the LAC for a particular type of glass, specifically by utilizing Lambert-Beer's law. This approach accurately measures the material's attenuation properties under controlled conditions.

$$\mu_{glass} = \frac{1}{x}\ln\left(\frac{I}{I_0}\right) \qquad (2)$$

The terms μ_{glass}, x, I_0, and I represent the thickness of the glass and the intensities of the incident and transmitted gamma rays, respectively.

The glass sample's half-value layer (HVL) refers to the thickness necessary to reduce the intensity of gamma ray photons to half of their original level. This measurement is determined via Equation (3) [23].

$$HVL(cm) = \frac{\ln(2)}{\mu_{glass}} \qquad (3)$$

Comprehending the HVL is vital for determining how effectively the glass shields against gamma radiation. The mass attenuation coefficient (MAC, expressed in cm^2/g) measures the probability of a photon interacting with a given material. It can be theoretically determined through the mixture rule.

The mass attenuation coefficient (MAC, expressed in cm^2/g) measures the probability of a photon interacting with a given material. It can be theoretically determined through the mixture rule. We can determine the MAC values via equation (4)

$$MAC = \mu_m = \frac{\mu}{\rho} \qquad (4)$$

The LAC values were calculated via the web-based programs referenced above. The difference (RD%) between the two calculated LAC values are evaluated via equation (5).

$$RD\ \% = \frac{(\mu)_{Phys-X} - (\mu)_{Py-MLBUF}}{(\mu)_{Phys-X}} \qquad (5)$$

The LAC values and relative deviation (RD%) over a comprehensive range of gamma-ray energies (0.015 MeV– 15 MeV) are shown in Table 2, and were derived from Phy-X/PSD and Py-MBLUF software

The effective atomic number (Z_{eff}) is another shielding parameter that can illustrate a multi element sample in relation to its equivalent element. The Z_{eff} for the invested glass samples can be derived via Eq. (6) [24].

$$Z_{eff} = \frac{\sigma_a}{\sigma_e} \qquad (6)$$

where

$$\sigma_a = \frac{1}{N_A} \sum_i f_i \, A_i (\mu_m)_i$$

$$\sigma_e = \frac{1}{N_A} \sum_i \frac{f_i A_i}{Z_i} (\mu_m)_i$$

According to the above equations, σ_a, σ_e, f_i, A_i, and Z_i represent the atomic cross section, electric cross section, fractional abundance, mass number, and atomic number of the i^{th} component of the studied glasses respectively.

Table 2. The Simulated and calculated linear attenuation coefficients (LACs) for the fabricated glasses.

Energy MeV	**Ag_2O 0%**			**Ag_2O 1%**			**Ag_2O 2%**		
	Phy-X/PSD cm^2/g	**Py-MLBUF** cm^2/g	**RD %**	**Phy-X/PSD** cm^2/g	**Py-MLBUF** cm^2/g	**RD %**	**Phy-X/PSD** cm^2/g	**Py-MLBUF** cm^2/g	**RD %**
0.015	187.881	188	0.031176267	189.445	190	0.028910105	190.414	190	0.029204695
0.02	132.524	133	0.002957544	133.200	133	0.000140285	133.460	133	0.000239427
0.03	46.486	46.5	0.01160703	48.043	48.0	0.009957424	49.444	49.4	0.009413215
0.04	34.567	34.6	0.005961562	35.285	35.3	0.007923433	35.890	35.9	0.007493772
0.05	19.412	19.4	0.003867333	19.805	19.8	0.004544278	20.135	20.1	0.003776454
0.06	12.128	12.1	0.001569335	12.367	12.4	0.00058812	12.567	12.6	0.003532355
0.08	5.841	5.84	0.0111442	5.950	5.95	0.008747497	6.040	6.04	0.009261207
0.1	8.826	8.83	0.00639518	8.881	8.88	0.006937513	8.908	8.91	0.006543477
0.15	3.292	3.29	0.012212323	3.311	3.31	0.012763707	3.320	3.32	0.014715828
0.2	1.712	1.71	0.022261656	1.723	1.72	0.018994553	1.727	1.73	0.022345067
0.3	0.777	7.77	0.001696726	0.782	0.782	1.07205E-05	0.784	0.784	0.000378068
0.4	0.499	0.499	0.012950121	0.503	0.503	0.013950847	0.505	0.505	0.013985761
0.5	0.379	0.379	0.012569754	0.382	0.382	0.011757919	0.383	0.383	0.010080485
0.6	0.313	0.313	0.011581148	0.316	0.316	0.011293638	0.317	0.317	0.011194035

0.8	0.244	0.244	0.004158505	0.246	0.246	0.003624949	0.247	0.247	0.003483389
1	0.206	0.206	0.004844317	0.208	0.208	0.004390204	0.209	0.209	6.29513E-05
1.5	0.159	0.159	0.000883054	0.161	0.161	0.005744814	0.162	0.162	0.001355555
2	0.139	0.139	0.008493482	0.141	0.141	0.004916868	0.141	0.141	0.002535315
3	0.122	0.122	0.012891174	0.123	0.123	0.009634927	0.123	0.123	0.011103469
4	0.114	0.114	0.001165678	0.116	0.116	0.000456553	0.116	0.116	0.003302462
5	0.111	0.111	0.001787803	0.113	0.113	0.002129463	0.113	0.113	0.001782277
6	0.111	0.111	0.001985592	0.112	0.112	0.002008828	0.113	0.113	0.004156199
8	0.112	0.112	0.005207149	0.113	0.113	0.008934991	0.114	0.114	0.006652157
10	0.115	0.115	0.004849844	0.116	0.116	0.005631976	0.117	0.117	0.000803481
15	0.124	0.124	0.000782966	0.125	0.125	0.000165824	0.127	0.127	0.004489268

3. Results and discussion.

The density of a material is regarded as a key physical parameter. Understanding the density of glass is essential for comprehending the changes in its structure as a result of dopant incorporation. To explore the structural alterations in glasses, it is imperative to measure their density, as any sudden variations in density can reveal significant structural changes that have taken place within the vitreous glass network.

The densities (ρ) and molar volumes (V_m) of the glasses (BBTLAg0-BBTLAg2) are shown in Fig. 1, highlighting their dependence on the Ag_2O mol% content. Additionally, as shown in Fig. 1 the density and molar volume of the fabricated glasses increased as the Ag_2O doping ratio increased.

Table 1 shows that glass sample BBTLA1 has a slight reduction in the molar volume (V_m) of the glass when the Ag_2O content is increased to 1%. This suggests that incorporating Ag_2O marginally reduces the interstitial spaces already present within the glass network. The substitution of the boron atom with a silver atom is attributed to the increase in density caused by the increased content of Ag_2O. Typically, density and molar volume exhibit opposing trends; however, this study presents an exception to that rule. Such abnormal behaviour has been previously reported in various glass systems, including TeO_2-ZnO-Er_2O_3 [23], B_2O_3-ZnO-TeO_2 [26], TeO_2-Bi_2O_3-ZnO-Na_2O-Nd_2O_3 [27], and [28], as well as by [29].

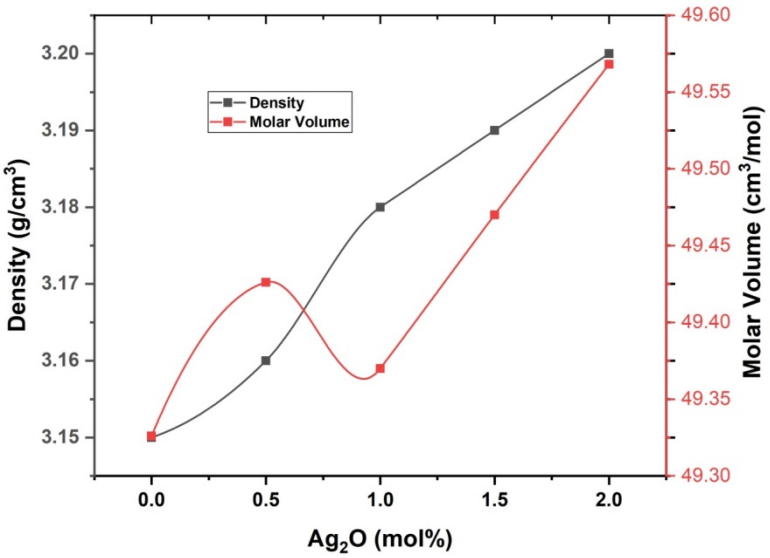

Fig. 1. Variation in the glass density and molar volume versus the doped Ag_2O ratio. Density and molar volume.

The increase in molar volume, due to the presence of nonbridging oxygen atoms (NBOs), results in bond breaking, consequently increasing the number of voids in the network [29]. The noted increase in molar volume could be attributed to either an increase in the bond length or an increase in the interatomic spacing between the atoms. The increase in the molar volume corresponding to the increase in the Ag_2O content can be attributed to various factors. One possible reason is that the ionic radius of the Ag^+ ions, which is 1.15 Å, is significantly larger than that of the B^{3+} ions (r = 0.27 Å) and Te^{4+} ions (r=0.97 Å). Ions with larger radii need more space, leading to an increase in the average bond length and a loosening of the packing of Ag^+ ions in the glass network [30]. Rather than enhancing packing, adding Ag_2O creates structural openness because of the larger size and modifying role of Ag^+ ions. Consequently, the molar volume increases.

3.1.Radiation Shielding Results

In this investigation, we analyzed the radiation attenuation performance of a selected glass system, TeO_2+B_2O_3+Bi_2O_3+La_2O_3+Ag_2O, by the determining shielding factors from 0.015 to 15 MeV. To perform these calculations, we utilized Phy-X software. The first parameter we calculate with respect to radiation shielding is the linear attenuation coefficient (LAC). Importantly high LAC values for particular media imply a strong ability to obstruct incoming photons. Therefore, this is significant for the development of effective shielding glass materials. The increase in LAC values corresponds with increasing Ag_2O concentration. At approximately 0.015 MeV, the LAC for all the fabricated glasses reached its highest values, which varied from 187.881 cm^{-1} to 190.414 cm^{-1} for BBTLAg0 and BBTLAg2, respectively.

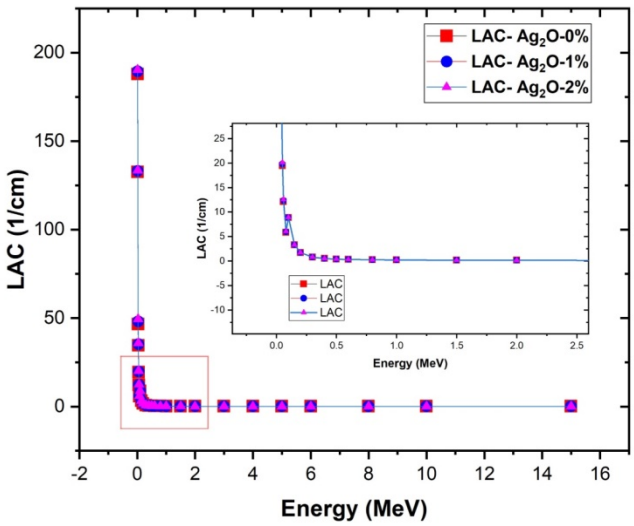

Fig. 2. For the prepared glasses, the linear attenuation coefficient was measured between 0.015 MeV and 15 MeV.

In Fig. 2, there was a significant reduction in LAC for all glass samples as the photon energy increased, because the interaction cross-section varied with $E^{-3.5}$ in PE mode. As shown in Fig. 2, the LAC values of 0%, 1%, and 2% Ag_2O glasses at 0.6 MeV were 0.313 cm^{-1}, 0.316 cm^{-1}, and 0.317 cm^{-1}, respectively. A significant increase in the LAC was observed at approximately 100 keV for all the manufactured glasses containing Ag_2O. This unusual increase could be attributed to the X-ray K-absorption edges of bismuth (Bi), which occur at 90.5 keV. For energies above 300 keV and extending to 6 MeV, the LAC values for all the designed glasses decrease progressively with increasing gamma photon energy. This could be associated with the Compton scattering interaction, which is most significant in this energy range. Above 4 MeV, the LAC values remained almost constant, likely because of the pair production process that occurs at high gamma ray energies. The LAC values at 15 MeV for glasses BBTLAg0 and BBTLAg2 range from 0.124 to 0.127 cm^{-1}, respectively.

The μ values for the glass samples studied at 0.6 MeV photon energy, which range from 0.313 to 0.317 cm^{-1}, are superior to those reported for the commercial glass samples RS-253 = 0.190 cm^{-1}, RS-253 G18 = 0.190 cm^{-1}, and RS-323 G19 = 0.280 cm^{-1}. Additionally, at 1 MeV, our glass has an LAC range of 0.206-0.209 cm^{-1} for the BBTLAg0-BBTLAg2 glass samples, which is better than those of RS-253 and RS-253 G18.

Table 3. Mass attenuation coefficients of the studied materials across the energy range of 0.015 MeV-15 MeV.

Energy (MeV)	**BBTLAg0**	**BBTLAg1**	**BBTLAg2**	**RS 253**	**OC**	**HS**	**BM**
0.015	59.645	59.574	59.504	7.478	7.054	21.536	20.575
0.02	42.071	41.887	41.706	3.312	3.105	9.660	9.208
0.03	14.757	15.108	15.451	1.116	1.1048	3.124	2.974
0.04	10.974	11.096	11.216	0.569	0.541	1.442	1.376
0.05	6.162	6.228	6.292	0.565	0.358	0.826	0.790
0.06	3.850	3.889	3.927	0.399	0.275	0.547	0.526
0.08	1.854	1.871	1.888	0.255	0.204	0.319	0.310
0.1	2.802	2.793	2.784	0.198	0.175	0.233	0.228
0.15	1.045	1.041	1.038	0.144	0.143	0.159	0.157
0.2	0.544	0.542	0.540	0.123	0.127	0.133	0.132
0.3	0.247	0.246	0.245	0.102	0.109	0.110	0.109
0.4	0.159	0.158	0.158	0.090	0.097	0.096	0.096
0.5	0.120	0.120	0.120	0.082	0.088	0.087	0.087
0.6	0.099	0.099	0.099	0.076	0.081	0.081	0.080
0.8	0.077	0.077	0.077	0.066	0.071	0.071	0.070
1	0.065	0.065	0.065	0.060	0.064	0.063	0.063
1.5	0.051	0.051	0.051	0.048	0.052	0.052	0.051
2	0.044	0.044	0.044	0.042	0.045	0.045	0.044
3	0.039	0.039	0.039	0.034	0.037	0.037	0.037
4	0.036	0.036	0.036	0.030	0.032	0.032	0.032
5	0.035	0.035	0.035	0.027	0.029	0.030	0.030
6	0.035	0.035	0.035	0.025	0.027	0.028	0.028
8	0.035	0.036	0.036	0.023	0.024	0.026	0.026
10	0.036	0.037	0.037	0.022	0.023	0.025	0.025
15	0.039	0.039	0.040	0.020	0.021	0.024	0.024

The mass attenuation coefficient (MAC), which is expressed in cm^2/g, reflects the probability of a photon interacting with a certain material. Table 3 shows the MAC values for all samples throughout the photon energy spectrum, ranging from 0.015 MeV to 15 MeV. Fig. 3 shows the connection between the MAC values and energy. It is evident that as the γ photon reaches 1 MeV, the MAC values decrease quickly. This decrease results from photoelectric absorption. This phenomenon is significant at low photon energy levels. It is generally acknowledged that the absorption cross-section related to the photoelectric effect varies with the material's atomic number, indicated as $Z^{4.5}$, and the energy of the primary photon, noted as $E^{-3.5}$. Thus, the MAC values for the glasses under investigation and the materials compared are at their peak in the low energy region [31].

Within the first region, across the initial gamma energy range of 015-0.02 MeV, the MAC values decrease as the amount of Ag_2O increases, which is attributed primarily to the leading photoelectric mechanism. The MAC values at 0.015 MeV are 59.645 cm^2/g, 59.574 cm^2/g, and 59.504 cm^2/g for Ag_2O at 0%, 1%, and 2%, respectively. The second region, which extends the gamma energy range of 0.03 MeV- 0.08 MeV suggests that the MAC values

increase as the Ag_2O fraction increases. Within the energy spectrum of 0.003 MeV- 0.08 MeV, the glass sample BBTLAg2 (2% Ag_2O) exhibited the highest MAC values, while the lowest MAC values were also noted in the ordinary concrete samples. As the molar percentage of the Ag_2O compound in the borotellurite glasses increased, the MAC values clearly increased, these findings indicate that glasses doped with Ag_2O possess superior absorption capacities compared with those of other materials.

At low photon energies such as 0.015 MeV, the interaction of photons is predominantly characterized by the photoelectric effect, which is strongly influenced by the atomic number (Z) of the elements involved and the electronic structure of the glass matrix. While silver (Ag, Z = 47) is a high-Z doping element in this study, Ag_2O is introduced in only small quantities (1- 2 mol%). It partially substitutes for heavier oxides such as TeO_2 (Z = 52) and Bi_2O_3 (Z = 83), which may result in a net reduction or minimal change in the effective atomic number (Z_{eff}) of the glass. Thus, a slight but consistent decrease in the MAC values at 0.015 MeV is noted with increasing Ag_2O content. This could be one of the reasons. As the energy increases, the MAC values for all the materials analyzed tend to be nearly equivalent within the energy range of approximately 0.5 MeV to 6 MeV. This is attributed to the dominance of Compton scattering in this energy range.

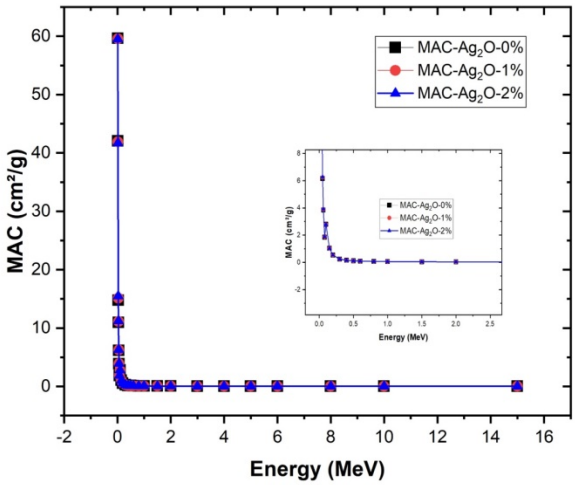

Fig. 3. Mass attenuation coefficients (μ/ρ) of the investigated glasses as a function of the photon energy.

The half-value and tenth-value layers signify the absorbance thickness needed to lower the photon flow by half and a tenth, respectively.

Fig. 4 and Fig. 5 depict the variation in HVL and MFP in the Ag_2O-doped boro-tellurite glass system as a function of the energy of the incident photons. An optimal radiation shielding material should possess lower MFP and HVL values. As illustrated in Figures 4 and 5, the values of HVL and MFP increase with increasing energy levels. In the low energy zone, these values approach zero. As shown in Fig. 4, we plotted the HVL for the BBTLAg glasses at specific energies. The data indicate that the HVL greatly influences the energy of the

radiation; thus, the thickness of the sample needed to attenuate the photons is dependent mainly on the radiation energy.

We have noted in our HVL and MFP values that at 0.1 MeV, there is a sharp decline in value rather than an increase. The drop in HVL and MFP at 0.1 MeV is due to a sudden rise in attenuation (LAC), likely caused by photoelectric edge (K-edge) absorption from the heavy elements in the glass under investigation. Specifically, this sudden decrease in HVL and MFP at 0.1 MeV is a consequence of the high LAC at this energy, as it is near the K-absorption edge of Bi, which occurs at 90.5 keV. After 0.1 MeV, the LAC again decreases, leading to the expected increase in HVL and MFP.

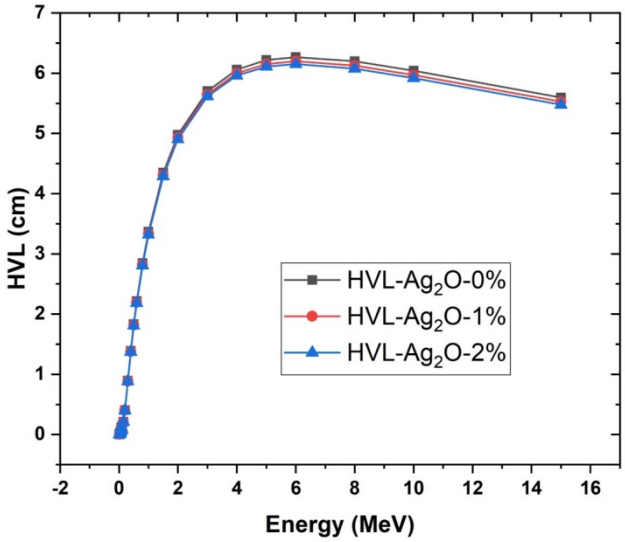

Fig. 4. The changes of half-value layers versus incident photon energy.

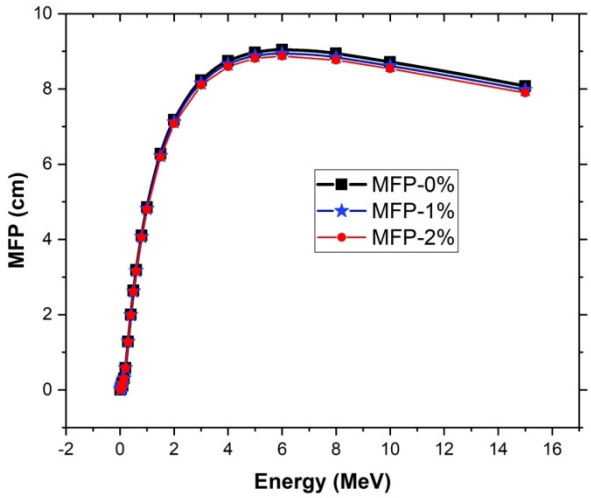

Fig. 5. The changes in Mean free paths versus incident photon energy.

Fig. 6, depicts consistent patterns in the effective atomic number (Z_{eff}) of all the glasses examined. The most noteworthy aspect of these trends is that the Z_{eff} values reach their

maximum at lower energy levels. We have also highlighted another essential parameter in radiation shielding, the effective atomic number (Z_{eff}). The effective atomic number (EAN), which is linked to the partial attenuation of photons, is valuable for evaluating a material's suitability for gamma applications. [32-34].

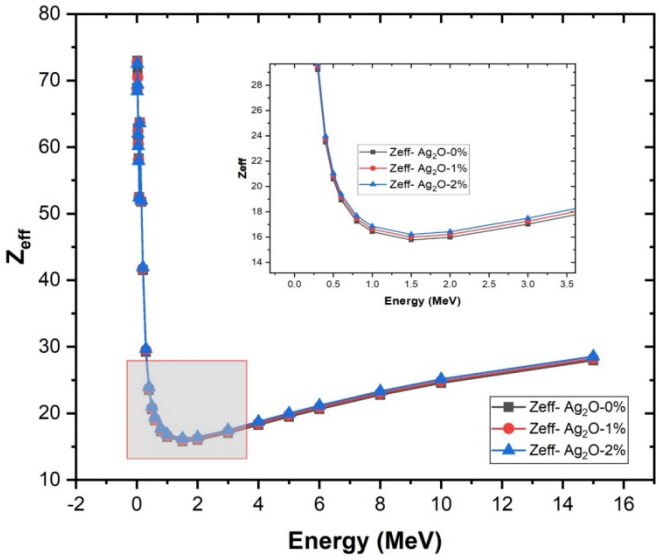

Fig. 6. Variation of effective atomic number (Z_{eff}) of Ag_2O 0%, Ag_2O 1%, and Ag_2O 2% of TeO_2+B_2O_3+Bi_2O_3+La_2O_3+Ag_2O glass systems as a function of incident photon energy (MeV).

As depicted in Fig. 6, the EAN (effective atomic number) of the TeO_2+B_2O_3+Bi_2O_3+La_2O_3+Ag_2O glass currently under study is presented as a function of energy, ranging from 0.015 MeV to 15 MeV. In the TeO_2+B_2O_3+Bi_2O_3+La_2O_3+Ag_2O glass systems, achieving a high Z_{eff} is beneficial for practical applications, which can be accomplished by selecting elements with relatively high atomic numbers. In the low energy range, the Z_{eff} values reach their peak for all glass samples, with the highest values occurring at the K absorption edges of the Bi element. As the energy increases to the middle and high energy ranges, the influence of energy on Z_{eff} decreases, and the lowest values are observed at high energies where pair production becomes predominant [35].

At 20 keV, the maximum EAN reached 72.95 for the Ag_2O-0% TeO_2+B_2O_3+Bi_2O_3+La_2O_3+Ag_2O glass. Nevertheless, the highest EAN values for the other samples were recorded at 30 keV, with values of approximately 70.46. At energies greater than 3 MeV, there is an apparent increase in Z_{eff}, which is driven mainly by the enhanced role of the Z^2-dependent pair production process. Table 4 contains the Z_{eff} values for all samples, allowing for a comprehensive evaluation. As illustrated in Fig. 6 and Table 3, our research indicates that the Z_{eff} values are greater in boro-tellurite glasses without Ag_2O doping than in other materials. This is particularly evident in the energy range where the photoelectric effect prevails. The hierarchy of Z_{eff} values throughout the whole energy range is BBTLAg0 > BBTLAg1 > BBTLAg2.

Table 4. The effective atomic numbers (Z_{eff}) of the analyzed materials in the energy interval of 0.015 MeV-15 MeV.

Energy (MeV)	**BBTLAg0**	**BBTLAg1**	**BBTLAg2**	**RS 253**	**OC**	**HS**	**BM**
0.015	68.90	68.65	68.40	15.354	13.789	21.911	21.376
0.02	72.95	72.74	72.54	15.316	13.585	21.767	21.283
0.03	71.65	70.46	69.38	14.729	12.754	20.806	20.489
0.04	62.79	62.38	61.99	13.794	11.730	19.223	19.130
0.05	60.78	60.46	60.16	17.619	10.849	17.419	17.548
0.06	58.31	58.09	57.89	15.972	10.207	15.730	16.042
0.08	52.47	52.46	52.45	13.603	9.469	13.205	13.748
0.1	63.69	63.62	63.56	12.264	9.121	11.713	12.369
0.15	51.75	51.87	51.98	10.900	8.810	10.161	10.917
0.2	41.52	41.73	41.93	10.462	8.718	9.668	10.452
0.3	29.22	29.46	29.71	10.187	8.662	9.361	10.162
0.4	23.49	23.73	23.97	10.103	8.644	9.269	10.075
0.5	20.57	20.81	21.04	10.068	8.637	9.231	10.038
0.6	18.93	19.16	19.39	10.050	8.633	9.211	10.019
0.8	17.24	17.46	17.69	10.033	8.629	9.191	10.001
1	16.42	16.64	16.86	10.024	8.627	9.182	9.991
1.5	15.78	16.00	16.21	10.022	8.630	9.186	9.996
2	15.99	16.21	16.43	10.036	8.648	9.232	10.038
3	17.03	17.26	17.49	10.087	8.709	9.383	10.177
4	18.25	18.50	18.75	10.148	8.783	9.566	10.345
5	19.48	19.74	20.00	10.210	8.860	9.757	10.520
6	20.64	20.92	21.19	10.272	8.939	9.948	10.694
8	22.75	23.04	23.33	10.388	9.088	10.31	11.018

						0	
10	24.55	24.84	25.14	10.490	9.222	10.632	11.305
15	27.94	28.25	28.55	10.688	9.488	11.266	11.859

4. CONCLUSION

This research outlines the radiation shielding parameters of Ag_2O-doped boro-tellurite integrated with bismuth and lanthanum oxides to determine their photon protection attributes. The calculations presented in this research were executed via Phy-X/PSD software.

The current investigation reveals that substituting B_2O_3 with Ag_2O induces considerable changes in the density and radiation shielding attributes of the (65-x) B_2O_3 + 15Bi_2O_3 + 15TeO_2 + 5La_2O_3 + xAg_2O glass system, where x is varied between 0 and 2 mol%

The changes in the MAC, LAC, HVL, MFP, and Z_{eff} for the current samples are shown within the energy range of 0.015 MeV to 15 MeV. A satisfactory evaluation was achieved by comparing these results with those of RS 253 glass and the concretes OC, BM, and HS. For radiation shielding purposes, the choice of an appropriate glass can be determined by LAC, HVL, and MFP data, along with the specific application in mind. Hence, BBTLAg2 glass is an excellent material for shielding against gamma rays and neutrons, outperforming competing shielding glasses and conventional concrete.

The radiation shielding capabilities of the synthesized glass samples were assessed by analyzing the effective atomic number (Z_{eff}), linear attenuation coefficient (LAC), mass attenuation coefficient (MAC), and HVL, MFP over an extensive energy range from 0.015 MeV to 15 MeV. Initially, the Z_{eff} values indicated that the glass without Ag_2O (0%) had the highest atomic number due to the presence of heavy oxides such as TeO_2 and Bi_2O_3. However, a more detailed examination of the MAC values, which offer a more precise measure of photon attenuation, revealed that glass samples with higher concentrations of Ag_2O, particularly at 2%, consistently achieved higher MAC values at low- and intermediate-energies. The greatest attenuation behaviour is noted at 0.015 MeV, and at this energy, we find that the MAC lies in the interval of 59.645 cm^2/g to 59.504 cm^2/g. According to the LAC results, BBTLAg2 (2%) showed the highest attenuation level among the samples due to Ag_2O.

According to the findings presented in this study, a sample containing 2 mol% Ag_2O has the most effective shielding properties, with the linear attenuation coefficient ranging from 12.567 cm^{-1} to 0.784 cm^{-1} as the gamma-ray energy increases from 0.06 to 3 MeV, respectively. In contrast to conventional concrete, RS-253, BBTLAg2 (2%) glass demonstrates enhanced gamma shielding properties over neutron shielding. Our research implies that bismuth boro-tellurite doped with Ag_2O glasses could be advantageous for protection against gamma, electron, and neutron radiation, allowing the Ag_2O and Bi_2O_3 contents to be modified according to the radiation type and energy. On the basis of the low HVL, TVL, and MFP values observed for the glass sample BBTLAg (2 mol%), this material is suggested to be an excellent γ-ray attenuator.

The investigation was confined to a Ag_2O concentration of 2 mol%; higher doping concentrations might reveal nonlinear trends in shielding performance. This study highlights that even minor increase in Ag_2O in boro-tellurite glass can subtly influence photon attenuation characteristics without significantly altering the transparency. This fine-tuned balance of shielding performance and optical clarity provides a unique opportunity to develop multifunctional radiation-protective materials that can serve structural, optical, and safety features, which is rarely accomplished in typical commercial glasses.

FUNDING

The authors are thankful for the financial support provided by the Vision Group on Science and Technology (VGST), Government of Karnataka, under the scheme KSTEPS/VGST/ECRA/GRD No. 1251/2023-24.

CONFLICT OF INTEREST

The authors declare that they have no conflicts of interest.

Decleration of generative AI use

Generative artificial intelligence (AI) tools were applied exclusively for the purpose of grammar and language refinement in the manuscript's preparation. The AI did not contribute to the research design, data collection, analysis, interpretation, or conclusions. The authors hold complete responsibility for all intellectual and scientific content.

5. REFERENCES

1. Willis, J.B., 1999. UNEP corner. Environ. Sci. Pollut. Res. 6(4), 192. https://doi.org/10.1007/bf02987324
2. Korkut, T., Umaç, Z.I., Aygün, B., Karabulut, A., Yapıcı, S., Şahin, R., 2013. Neutron equivalent dose rate measurements of Gypsum–Waste tire rubber layered structures. Int. J. Polym. Anal. Charact. 18(6), 423–429. https://doi.org/10.1080/1023666x.2013.814025.
3. Naseer, A., Marimuthu, K., Mahmoud, K.A., Sayyed, M.I., 2021. Impact of Bi**2**O**3** modifier concentration on barium–zinc borate glasses: physical, structural, elastic, and radiation-shielding properties. Eur. Phys. J. Plus 136, 41. https://doi.org/10.1140/epjp/s13360-020-01056-6

4. Prasad, R., Pai, A.R., Oyadiji, S.O., Thomas, S., Parashar, S., 2022. Utilization of hazardous red mud in silicone rubber/MWCNT nanocomposites for high performance electromagnetic interference shielding. J. Clean. Prod. 377, 134290. https://doi.org/10.1016/j.jclepro.2022.134290
5. Şahin, N., Bozkurt, M., Karabul, Y., Kılıç, M., Özdemir, Z.G., 2021. Low cost radiation shielding material for low energy radiation applications: Epoxy/Yahyali Stone composites. Prog. Nucl. Energy 135, 103703. https://doi.org/10.1016/j.pnucene.2021.103703
6. Agar, O., Khattari, Z.Y., Sayyed, M.I., Tekin, H.O., Al-Omari, S., Maghrabi, M., Zaid, M.H.M., Kityk, I.V., 2019. Evaluation of the shielding parameters of alkaline earth-based phosphate glasses using MCNPX code. Results Phys. 12, 101–106. https://doi.org/10.1016/j.rinp.2018.11.054.
7. Al-Hadeethi, Y., Sayyed, M.I., Mohammed, H., Rimondini, L., 2020. X-ray photons attenuation characteristics for two tellurite based glass systems at dental diagnostic energies. Ceram. Int. 46, 251–257. https://doi.org/10.1016/j.ceramint.2019.08.258
8. Rashad, M., Ali, A.M., Sayyed, M.I., Somaily, H.H., Algarni, H., Rammah, Y.S., 2020. Radiation attenuation and optical features of lithium borate glasses containing barium: B_2O_3–Li_2O–BaO. Ceram. Int. 46, 21000–21007. https://doi.org/10.1016/j.ceramint.2020.05.165
9. Sayyed, M.I., Tekin, H.O., Kılıcoglu, O., Agar, O., Zaid, M.H.M., 2018. Shielding features of concrete types containing sepiolite mineral: comprehensive study on experimental, XCOM and MCNPX results. Results Phys. 11, 40–45. https://doi.org/10.1016/j.rinp.2018.08.029
10. Ersundu, Ç., Ersundu, A.E., Kityk, I.V., 2018. Investigation on gamma and neutron radiation shielding parameters for BaO/SrO–Bi_2O_3–B_2O_3 glasses. Radiat. Phys. Chem. 145, 26–33. https://doi.org/10.1016/j.radphyschem.2017.12.010
11. Boukhris, I., Kebaili, I., Al-Buriahi, M., Tonguc, B., AlShammari, M.M., Sayyed, M.I., 2020. Effect of bismuth oxide on the optical features and gamma shielding efficiency of lithium zinc borate glasses. Ceram. Int. 46(14), 22883–22888. https://doi.org/10.1016/j.ceramint.2020.06.061
12. Mhareb, M., Alajerami, Y., Dwaikat, N., Al-Buriahi, A.M., Alshahri, F., Saleh, N., Alonizan, N., Saleh, M., Sayyed, M.I., 2020. Investigation of photon, neutron and proton shielding features of H_2BO_3–ZnO–Na_2O–BaO glass system. Nucl. Eng. Technol. 53(3), 949–959. https://doi.org/10.1016/j.net.2020.07.035
13. Mahmoud, K., Rammah, Y., 2019. Investigation of gamma-ray shielding capability of glasses doped with Y, Gd, Nd, Pr and Dy rare earth using MCNP-5 code. Physica B 577, 411756. https://doi.org/10.1016/j.physb.2019.411756.
14. Lakshminarayana, G., Elmahroug, Y., Kumar, A., Rekik, N., Lee, D., Yoon, J., Park, T., 2020. Reckoning of nuclear radiation attenuation capabilities for binary GeO_2–Tl_2O, GeO_2–Bi_2O_3, and ternary GeO_2–Tl_2O–Bi_2O_3 glasses utilizing pertinent theoretical and computational approaches. Opt. Mater. 108, 110113. https://doi.org/10.1016/j.optmat.2020.110113

15. Abdelghany, Y., Kassab, M., Radwan, M., Abdel-Latif, M., 2022. Borotellurite glass system doped with ZrO_2, potential use for radiation shielding. Prog. Nucl. Energy 149, 104256. https://doi.org/10.1016/j.pnucene.2022.104256
16. Halimah, M., Azuraida, A., Ishak, M., Hasnimulyati, L., 2019. Influence of bismuth oxide on gamma radiation shielding properties of boro-tellurite glass. J. Non-Cryst. Solids 512, 140–147. https://doi.org/10.1016/j.jnoncrysol.2019.03.004
17. Rammah, Y., 2020. Influence of Ag_2O insertion on alpha, proton and γ-rays safety features of TeO_2–ZnO–Na_2O glasses: potential use for nuclear medicine applications. Ceram. Int. 46(11), 18151–18159. https://doi.org/10.1016/j.ceramint.2020.04.136
18. Ennouri, M., Kuusela, L., Jlassi, I., Gelloz, B., Petit, L., Elhouichet, H., 2019. Impact of Ag_2O content on the optical and spectroscopic properties of fluoro-phosphate glasses. Mater. 12(21), 3516. https://doi.org/10.3390/ma12213516
19. Kumar, R.P., Lenkennavar, S.K., 2024. An investigation into empirical equations for predicting density and packing density parameters across diverse chemical compositions: a theoretical approach. Prabha Mater. Sci. Lett. 4(1), 66–77. https://doi.org/10.33889/pmsl.2025.4.1.006
20. Şakar, E., Özpolat, Ö.F., Alım, B., Sayyed, M., Kurudirek, M., 2019. Phy-X/PSD: Development of a user friendly online software for calculation of parameters relevant to radiation shielding and dosimetry. Radiat. Phys. Chem. 166, 108496. https://doi.org/10.1016/j.radphyschem.2019.108496
21. Aloraini, D.A., Almuqrin, A.H., Sayyed, M.I., Kumar, A., Gaikwad, D., Tishkevich, D.I., Trukhanov, A., 2021. Experimental and theoretical analysis of radiation shielding properties of strontium-borate-tellurite glasses. Opt. Mater. 121, 111589. https://doi.org/10.1016/j.optmat.2021.111589
22. Mann, K.S., Mann, S.S., 2020. Py-MLBUF: Development of an online-platform for gamma-ray shielding calculations and investigations. Ann. Nucl. Energy 150, 107845. https://doi.org/10.1016/j.anucene.2020.107845
23. Rammah, Y.S., Sayyed, M.I., Ali, A.A., Tekin, H.O., El-Mallawany, R., 2018. Optical properties and gamma-shielding features of bismuth borate glasses. Appl. Phys. A 124, 815. https://doi.org/10.1007/s00339-018-2252-7
24. Mansour, A., Sayyed, M.I., Mahmoud, K.A., Şakar, E., Kovaleva, E.G., 2020. Modified halloysite minerals for radiation shielding purposes. J. Radiat. Res. Appl. Sci. 13(1), 94–101. https://doi.org/10.1080/16878507.2019.1699680
25. Nazrin, S., Halimah, M., Muhammad, F., Yip, J., Hasnimulyati, L., Faznny, M., Hazlin, M., Zaitizila, I., 2018. The effect of erbium oxide in physical and structural properties of zinc tellurite glass system. J. Non-Cryst. Solids 490, 35–43. https://doi.org/10.1016/j.jnoncrysol.2018.03.017
26. Marzuki, A., Djeksadipura, W.M.S., Suryanti, V., Fausta, D.E., Saraswati, A., Singgih, G.T., 2021. Compositional dependence of density and refractive index in borotellurite glass. J. Phys. Conf. Ser. 1912(1), 012026. https://doi.org/10.1088/1742-6596/1912/1/012026
27. Marzuki, A., Pramuda, A., Fausta, D.E., 2020. Effect of Nd_2O_3 and Na_2O concentration on physical and spectroscopic properties of TeO_2–Bi_2O_3–ZnO–Na_2O–

Nd_2O_3 glasses. Mater. Res. Express 7(6), 065201. https://doi.org/10.1088/2053-1591/ab8b89

28. Rajendran, V., Palanivelu, N., Chaudhuri, B., Goswami, K., 2003. Characterisation of semiconducting V_2O_5–Bi_2O_3–TeO_2 glasses through ultrasonic measurements. J. Non-Cryst. Solids 320(1–3), 195–209. https://doi.org/10.1016/s0022-3093(03)00018-8
29. Saddeek, Y.B., Latif, L.E., 2004. Effect of TeO_2 on the elastic moduli of sodium borate glasses. Physica B 348(1–4), 475–484. https://doi.org/10.1016/j.physb.2004.02.001
30. Pascuta, P., Pop, L., Rada, S., Bosca, M., Culea, E., 2007. The local structure of bismuth borate glasses doped with europium ions evidenced by FT-IR spectroscopy. J. Mater. Sci. Mater. Electron. 19(5), 424–428. https://doi.org/10.1007/s10854-007-9359-5
31. Alim, B., 2020. Determination of radiation protection features of the Ag_2O doped Boro-Tellurite glasses using Phy-X/PSD software. Iğdır Univ. J. Inst. Sci. Technol. 10(1), 202–213. https://doi.org/10.21597/jist.640027
32. Al-Buriahi, M.S., Arslan, H., Tonguç, B.T., 2019. Mass attenuation coefficients, water and tissue equivalence properties of some tissues by Geant4, XCOM and experimental data. Indian J. Pure Appl. Phys. 57(6), 433–437.
33. Al-Buriahi, M.S., Tekin, H.O., Kavaz, E., Tonguc, B.T., Rammah, Y.S., 2019. New transparent rare earth glasses for radiation protection applications. Appl. Phys. A 125, 930. https://doi.org/10.1007/s00339-019-3077-8
34. Zakaly, H.M., Saudi, H., Issa, S.A., Rashad, M., Elazaka, A., Tekin, H., Saddeek, Y.B., 2020. Alteration of optical, structural, mechanical durability and nuclear radiation attenuation properties of barium borosilicate glasses through BaO reinforcement: experimental and numerical analyses. Ceram. Int. 47(4), 5587–5596. https://doi.org/10.1016/j.ceramint.2020.10.143
35. Gaballah, M., Issa, S.A.M., Saddeek, Y.B., Elsaman, R., Susoy, G., Erguzel, T.T., Alharbi, T., Tekin, H.O., 2020. Mechanical and nuclear radiation shielding properties of different boro-tellurite glasses: a comprehensive investigation on large Bi_2O_3 concentration. Phys. Scr. 95(8), 085701. https://doi.org/10.1088/1402-4896/ab9bde